hepatic glucose phosphorylation by an AMP-activated protein kinase-independent effect on glucokinase translocation. Diabetes 55:865–874
34. Hinke SA, Martens GA, Cai Y et al (2007) Methyl succinate antagonises biguanide-induced AMPK-activation and death of pancreatic beta-cells through restoration of mitochondrial electron transfer. Br J Pharmacol 150:1031–1043
35. Zhang L, He H, Balschi JA (2007) Metformin and phenformin activate AMP-activated protein kinase in the heart by increasing cytosolic AMP concentration. Am J Physiol Heart Circ Physiol 293:H457–H466
36. Bashan N, Kovsan J, Kachko I, Ovadia H, Rudich A (2009) Positive and negative regulation of insulin signaling by reactive oxygen and nitrogen species. Physiol Rev 89:27–71

Exendin-4 Protects Pancreatic Beta Cells from the Cytotoxic Effect of Rapamycin by Inhibiting JNK and p38 Phosphorylation

Authors Y. Kawasaki[1], S. Harashima[1], M. Sasaki[1], E. Mukai[1,2], Y. Nakamura[1], N. Harada[1], K. Toyoda[1], A. Hamasaki[1], S. Yamane[1], C. Yamada[1], Y. Yamada[1,3], Y. Seino[1,4], N. Inagaki[1,5]

Affiliations Affiliation addresses are listed at the end of the article

Key words
- exendin-4
- rapamycin
- JNK
- p38
- beta cells

Abstract

It has been reported that the immunosuppressant rapamycin decreases the viability of pancreatic beta cells. In contrast, exendin-4, an analogue of glucagon-like peptide-1, has been found to inhibit beta cell death and to increase beta cell mass. We investigated the effects of exendin-4 on the cytotoxic effect of rapamycin in beta cells. Incubation with 10 nM rapamycin induced cell death in 12 h in murine beta cell line MIN6 cells and Wistar rat islets, but not when coincubated with 10 nM exendin-4. Rapamycin was found to increase phosphorylation of c-Jun amino-terminal kinase (JNK) and p38 in 30 minutes in MIN6 cells and Wistar rat islets while exendin-4 decreased their phosphorylation. Akt and extracellular signal-regulated kinase (ERK) were not involved in the cytoprotective effect of exendin-4. These results indicate that exendin-4 may exert its protective effect against rapamycin-induced cell death in pancreatic beta cells by inhibiting JNK and p38 signaling.

received 19.09.2009
accepted 08.02.2010

Bibliography
DOI http://dx.doi.org/10.1055/s-0030-1249035
Published online: 2010
Horm Metab Res
© Georg Thieme Verlag KG Stuttgart · New York
ISSN 0018-5043

Correspondence
N. Inagaki, MD, PhD
Department of Diabetes and Clinical Nutrition
Graduate School of Medicine
Kyoto University
54 Shogoin Kawahara-cho
Sakyo-ku
606-8507 Kyoto
Japan
Tel.: +81/75/751 3560
Fax: +81/75/771 6601
inagaki@metab.kuhp.kyoto-u.ac.jp

Introduction

Exendin-4 is presently being used in patients with type 2 diabetes [1]. The glucagon-like peptide-1 (GLP-1) analogue improves blood glucose levels by increasing insulin secretion. Exendin-4 is also suggested to promote beta cell proliferation and neogenesis and to inhibit beta cell apoptosis, thereby increasing beta cell mass, at least in rodents [2]. Apoptosis induced by inflammatory cytokines [3] or endoplasmic reticulum (ER) stress [4] was shown to be prevented by exendin-4 in primary rat beta cells and INS-1, a murine beta cell line. Treatment with exendin-4 markedly attenuates beta cell apoptosis in db/db mice [5] and in male C57BL/6 mice exposed to streptozotocin [6]. The molecular mechanism of the cytoprotective effect of exendin-4 is mediated by increased levels of cyclic AMP (cAMP) that lead to activation of protein kinase A (PKA), enhanced insulin receptor substrate-2 (IRS-2) activity, and activation of Akt and extracellular signal-regulated kinase (ERK) [7]. Recently it was reported that exendin-4 inhibits cytokine-induced apoptosis, which involves electron transport chain proteins of mitochondria with a reduction of oxidative stress in INS-1 cells [8].

Rapamycin, an immunosuppressant used to prevent rejection in organ transplantation, is reported to impair glucose-stimulated insulin secretion in rat islets and to decrease viability of rat and human islets [9]. A recent study suggested that rapamycin reduces beta cell mass by 50% under diabetic conditions in *Psammomys obesus*, an animal model of nutrition-dependent type 2 diabetes, by increasing c-Jun amino-terminal kinase (JNK) phosphorylation [10].

We investigated whether exendin-4 might ameliorate the cytotoxic effects of rapamycin. In the present study, we found that rapamycin induces cell death in beta cells through an increase in phosphorylation of JNK and p38, and that exendin-4 prevents such rapamycin-induced cell death by inhibiting these molecules.

Materials and Methods

Materials

Tissue culture media, DMEM and RPMI1640, rapamycin, exendin-4, exendin (9–39) (exendin-9), H89, LY294002, PD98059, SP600125, SB203580, RNaseA, propidium iodide (PI), and anti-α-tubulin antibody (Ab) were obtained from Sigma Aldrich (St Louis, MO, USA). Fetal bovine

serum (FBS) was from Invitrogen (Carlsbad, CA, USA). Anti-phospho-Akt (Ser473) Ab, anti-Akt Ab, anti-phospho-JNK (Thr183/Tyr185) Ab, anti-JNK Ab, anti-phospho-p38 (Thr180/Tyr182) Ab, anti-p38 Ab, anti-caspase-3 Ab, and anti-cleaved caspase-3 Ab were obtained from Cell Signaling (Danvers, MA, USA). Anti-phospho-ERK Ab and anti-ERK Ab were from Santa Cruz Biotechnology (Santa Cruz, CA, USA).

Methods

Cell culture and stimulation of MIN6 cells

MIN6 cells were maintained in 25 mM glucose DMEM media supplemented with 13% FBS, 100U/ml penicillin, 100µg/ml streptomycin, and 5µl β-mercaptoethanol at 37°C in humidified air containing 5% CO_2. For the experiment, the cells (1.2×10^6) were plated into 35 mm dishes, incubated in DMEM media with or without protein kinase inhibitors for 30 min, and rapamycin and/or exendin-4, and/or forskolin, and/or exendin-9 were then added into the media. After the indicated time periods, the cells were collected and analyzed for cell death and protein phosphorylation.

Islet isolation and stimulation

Pancreatic islets were isolated from Wistar rats by collagenase digestion as described previously [11], and preincubated in RPMI 1640 medium containing 10% FBS, 100U/ml penicillin, 100µg/ml streptomycin, and 5.5 mM glucose at 37°C in humidified air containing 5% CO_2 for 60 min. After preincubation, the islets were cultured in the media with 10 nM rapamycin and/or 10 nM exendin-4 for the indicated time periods and then analyzed for cell death, protein phosphorylation, and insulin secretion and content.

Insulin secretion and content

Insulin secretion from islets was monitored using batch incubation as previously described [11]. After islets were cultured with 10 nM rapamycin and/or 10 nM exendin-4 for 12 h, the islets were collected, washed, and preincubated at 37°C for 30 min in Krebs-Ringer bicarbonate buffer (KRBB) medium supplemented with 2.8 mM glucose, and groups of 5 islets were then batch-incubated for 30 min in 0.7 ml KRBB medium containing 2.8 mM and 16.7 mM glucose. At the end of the incubation period, the islets were pelleted by centrifugation, and aliquots of the buffer were sampled to determine the amount of immunoreactive

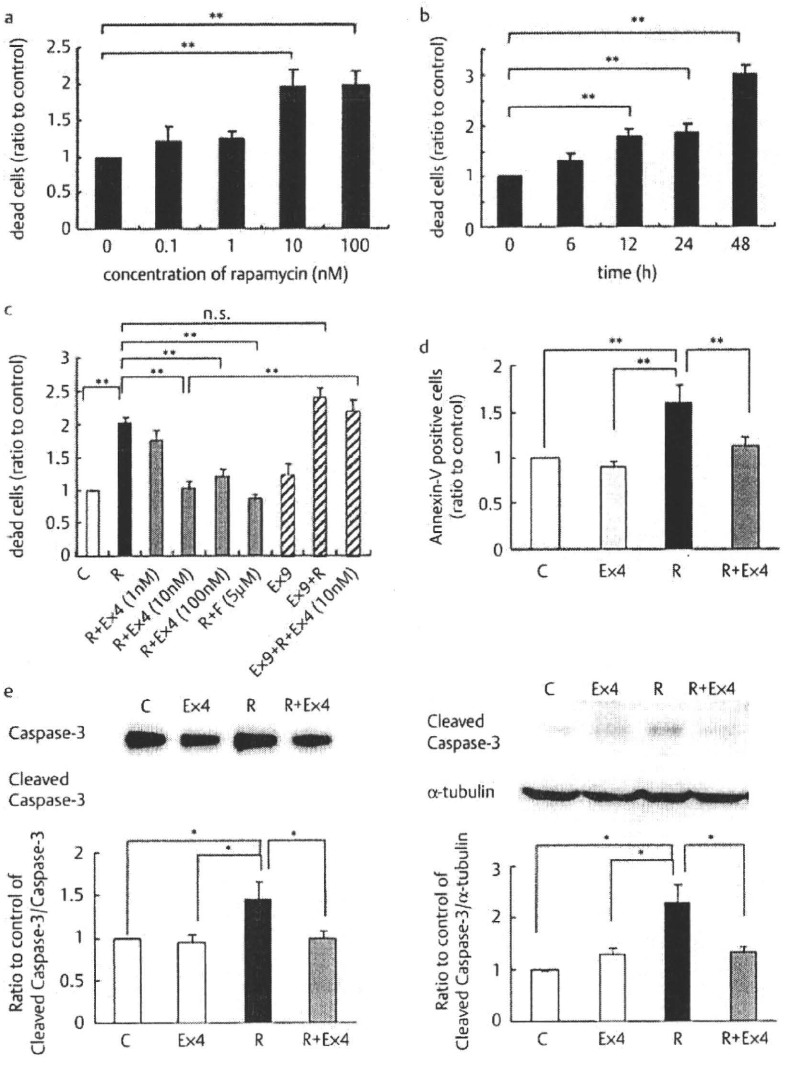

Fig. 1 Exendin-4 inhibits rapamycin-induced cell death in MIN6 cells. **a**: Dose-dependency and **b**: time-dependency of rapamycin-induced cell death in MIN6 cells. MIN6 cells were treated with 0.1, 1, 10, or 100 nM rapamycin for 12 h (**a**) or with 10 nM rapamycin for 6, 12, 24, or 48 h (**b**), and dead cells with sub-G1 DNA content were counted by flowcytometer. Data are means ± SE of five independent experiments. ** $p < 0.01$.
c: Quantification of dead cells 12 h after treatment with DMSO (control), 10 nM rapamycin, 10 nM rapamycin and 1, 10, or 100 nM exendin-4, 10 nM rapamycin and 5 µM forskolin, 100 nM exendin-9, and 100 nM exendin-9 and 10 nM rapamycin with or without 10 nM exendin-4. Data are means ± SE of four independent experiments. ** $p < 0.01$. **d**: The percentage of annexin-V-FITC positive cells. MIN6 cells were cultured with 10 nM rapamycin and/or 10 nM exendin-4, and annexin-V-FITC positive cells were counted by flowcytometer. Data are means ± SE of three independent experiments. ** $p < 0.01$. **e**: Western blot analysis of caspase-3 and cleaved caspase-3 in MIN6 cells treated with 10 nM rapamycin and/or 10 nM exendin-4 for 12 h. Images are representative of three independent experiments. Graphs show relative ratio of cleaved caspase-3 versus caspase-3 or α-tubulin, respectively. * $p < 0.05$. C: control (DMSO); R: rapamycin; Ex4: exendin-4; F: forskolin; Ex9: exendin-9.

insulin by RIA. After an aliquot of incubation medium for insulin release assay in 2.8 mM glucose was taken, the remaining islets were lysed and insulin contents were determined.

Quantification of cell death

MIN6 cells incubated under the conditions indicated were collected from both attached and floating cell populations and fixed with 70% ethanol for 4 h. The cells were then washed with PBS, incubated in phosphate-citrate buffer for 30 min, resuspended in 10 µg/ml RNaseA containing PBS, and stained with 10 µg/ml PI. Dead cells containing sub-G1 DNA content were identified and analyzed by a FACS Calibur instrument (BD Biosciences, San Jose, CA, USA). Annexin-V positive cells were analyzed by FACS Calibur using annexin-V-FITC Apoptosis Detection Kit (BD Pharmingen, San Diego, CA, USA). Primary islets were cultured in the indicated conditions for 12 h. DNA fragmentation was measured by quantification of cytosolic oligonucleosome-bound DNA using Cell Death Detection ELISA (Roche, Mannheim, Germany) as previously described [12]. To detect caspase-3 activity, MIN6 cells and primary islets were cultured with 10 nM rapamycin and/or 10 nM exendin-4 for 12 h, and 50 µg of the proteins were subjected to western blot analysis.

Western blot analysis

Cells were collected and washed twice with PBS, and then sonicated in lysis buffer. Equivalent amounts of protein were resolved by SDS/PAGE on 4–12% acrylamide gels (Invitrogen) and transferred to PVDF membranes (Invitrogen), followed by immunoblotting with antibodies to detect respective proteins.

Fluorescence labeling with Newport Green

Islet beta cells from Wistar rat were cultured with 10 nM rapamycin and/or 10 nM exendin-4 for 12 h and stained with Newport Green (Invitrogen) for 30 min. The labeled beta cells were visualized by fluorescence microscopy (Keyence, New Jersey, USA).

Statistics

Data are expressed as mean ± SE. Statistical comparisons were made between groups using one-way analysis of variance. Significant differences were evaluated using Tukey-Kramer post hoc analysis.

Results

Exendin-4 inhibits rapamycin-induced cell death in MIN6 cells

We first examined the dose-dependency and time-dependency of rapamycin-induced cell death in MIN6 cells. The number of dead cells was significantly increased in 10 and 100 nM rapamycin-treated MIN6 cells compared to that in DMSO-treated cells (control) in 12 h (◎ **Fig. 1a**). The number of dead cells induced by 10 nM rapamycin, a therapeutic concentration in blood [13], was significantly increased from 12 h and maximized at 48 h (◎ **Fig. 1b**), indicating cytotoxicity in MIN6 cells in 12 h.

MIN6 cells were then treated with 1, 10, or 100 nM exendin-4 in the presence of 10 nM rapamycin for 12 h. The number of rapamycin-induced dead cells was significantly reduced by 97.0 ± 14.9% and 78.1 ± 14.5% by coincubation with 10 and 100 nM exendin-4, respectively (◎ **Fig. 1c**). In addition, 5 µM forskolin, an adenylyl cyclase activator, completely blocked rapamycin-induced cell death (◎ **Fig. 1c**). In addition, exendin-9, an

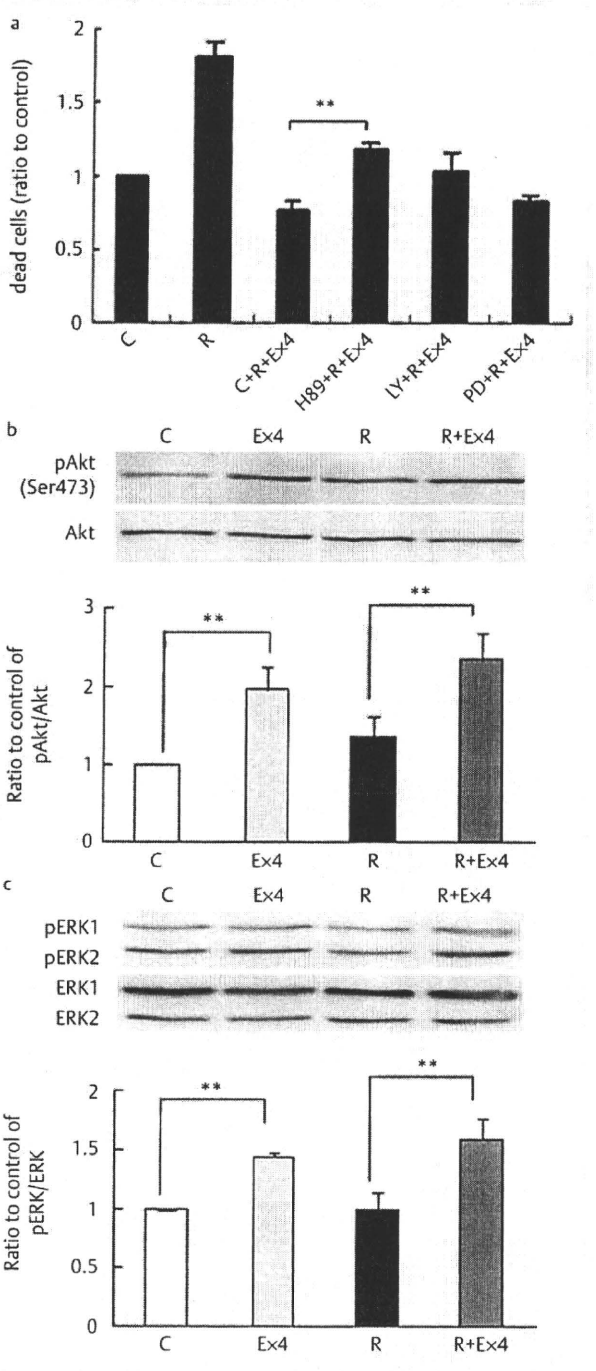

Fig. 2 Cytoprotective effect of exendin-4 is partially mediated by PKA, but not by PI3K/Akt and ERK. **a**: The percentage of dead cells with sub-G1 DNA content. DMSO (control), 15 µM H89, 10 µM LY294002, or 50 µM PD98059 was added into the media 30 min before treatment with 10 nM rapamycin and 10 nM exendin-4 for 12 h in MIN6 cells, and dead cells were counted by flowcytometer. Data are means ± SE of four independent experiments. ** $p < 0.01$. **b**, **c**: Western blot analysis of Akt and ERK in MIN6 cells treated with 10 nM rapamycin and/or 10 nM exendin-4 for 30 min. Images are representative of three independent experiments. Graphs show relative ratio of phosphorylated Akt or ERK vs. total Akt or ERK, respectively, by treatment with rapamycin and/or exendin-4 compared to control (DMSO). Data are means ± SE of three independent experiments. ** $p < 0.01$. C: control (DMSO); R: rapamycin; Ex4: exendin-4; LY: LY294002; PD: PD98059.

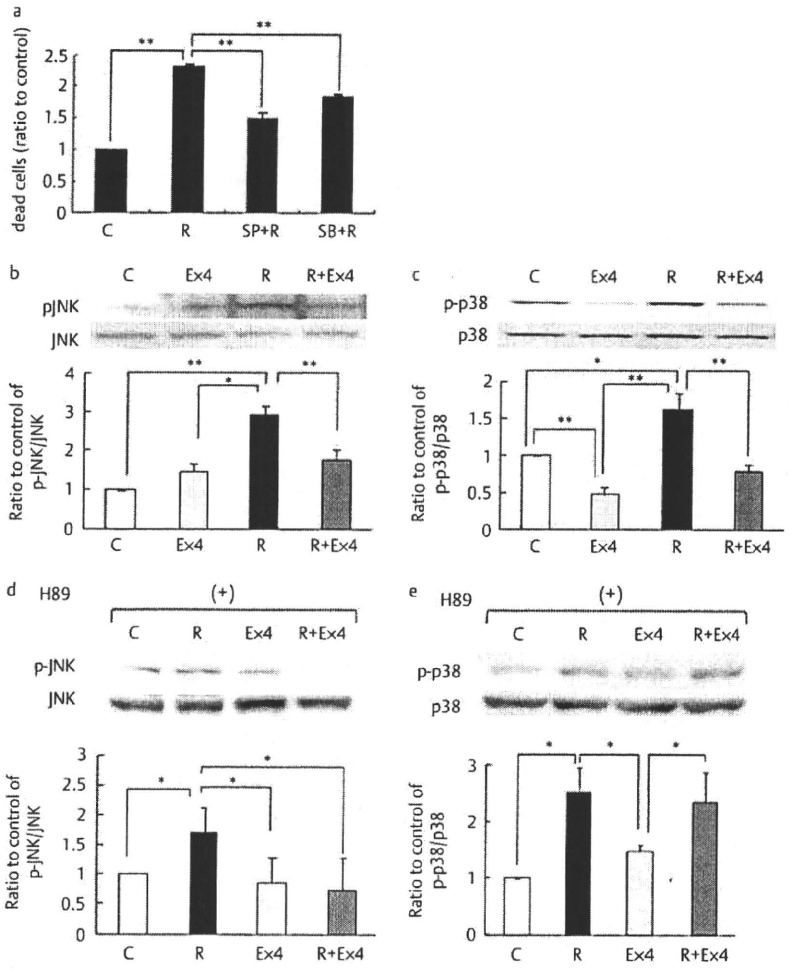

Fig. 3 Exendin-4 inhibits rapamycin-induced cell death by decreasing JNK and p38 phosphorylation in MIN6 cells. **a:** The percentage of dead cells with sub-G1 DNA content. DMSO (control), 10 μM SP600125 or 10 μM SB203580 was added into MIN6 cells 30 min before treatment with 10 nM rapamycin for 12 h, and dead cells were counted by flowcytometer. Data are means ± SE of four independent experiments. ** $p<0.01$.
b, c: Western blot analysis of JNK and p38 in MIN6 cells treated with 10 nM rapamycin and/or 10 nM exendin-4 for 30 min. **d, e:** Western blot analysis of JNK and p38 in MIN6 cells to which 15 μM H89 was added 30 min before incubation with 10 nM rapamycin and/or 10 nM exendin-4 for 30 min. Images are representative of three independent experiments. Graphs show relative ratio of phosphorylated JNK or p38 v.s. total JNK or p38, respectively, by treatment with rapamycin and/or exendin-4 compared to control (DMSO). Data are means ± SE of three independent experiments. * $p<0.05$ ** $p<0.01$. C: control (DMSO); R: rapamycin; Ex4: exendin-4; SP: SP600125; SB: SB203580.

antagonist of the GLP-1 receptor, inhibited the cytoprotective effect of exendin-4 on rapamycin-induced cell death (○ **Fig. 1c**). Annexin-V-positive apoptotic cells were also significantly increased in rapamycin-treated MIN6 cells compared to those in control cells, which increase was prevented by treatment with exendin-4 (○ **Fig. 1d**). Furthermore, rapamycin increased caspase-3 activity, while exendin-4 decreased it in rapamycin-treated MIN6 cells (○ **Fig. 1e**). These results indicate that exendin-4 inhibits rapamycin-induced cell death through the GLP-1 receptor by an increase in the intracellular cAMP concentration in MIN6 cells.

Cytoprotective effect of exendin-4 is mediated in part by PKA, but not by PI3K and ERK

We then examined the involvement of PKA, phosphatidylinositol 3-kinase (PI3 K)/Akt, and ERK, downstream molecules of the GLP-1 receptor signaling pathways. DMSO (control), 15 μM H89, a PKA inhibitor, 10 μM LY294002, a PI3 K inhibitor, or 50 μM PD98059, an ERK inhibitor, was added into the media 30 min before treatment with 10 nM exendin-4 and 10 nM rapamycin for 12 h in MIN6 cells, and dead cells were counted by flowcytometer. H89, a PKA inhibitor, partially but significantly blocked the cytoprotective effect of exendin-4 (○ **Fig. 2a**). On the other hand, neither LY294002 nor PD98059 altered the cytoprotective effect of exendin-4 against rapamycin-induced cell death (○ **Fig. 2a**), although phosphorylation of Akt and ERK was significantly increased by treatment with exendin-4 (○ **Fig. 2b** and **c**). These results indicate that PKA is involved, at least in part, in the cytoprotective effect of exendin-4 against rapamycin-induced cell death.

JNK and p38 are involved in rapamycin-induced cell death in MIN6 cells

Previous studies found that rapamycin induces apoptosis in rh30, a human rhabdomyosarcoma cell line [14], and in islets isolated from *P. Obesus* [10], by activating JNK. In contrast, rapamycin inhibits palmitate-induced ER stress and apoptosis in INS-1E cells [15]. To clarify the involvement of JNK in rapamycin-induced cytotoxicity in MIN6 cells, 10 μM SP600125, a JNK inhibitor, was added into the media 30 min before treatment with 10 nM rapamycin for 12 h, when dead cells were counted by flowcytometer. SP600125 significantly inhibited rapamycin-induced cell death by 62.6 ± 9.1 % (○ **Fig. 3a**). We also examined the involvement of p38, the other stress-activated protein kinase [16]. Ten μM SB203580, a p38 inhibitor, added to MIN6 cells 30 min before treatment with 10 nM rapamycin for 12 h resulted in significant inhibition of rapamycin-induced cell death by 36.8 ± 6.4 % (○ **Fig. 3a**). These results indicate that rapamycin-induced cell death is mediated by JNK and p38 in MIN6 cells.

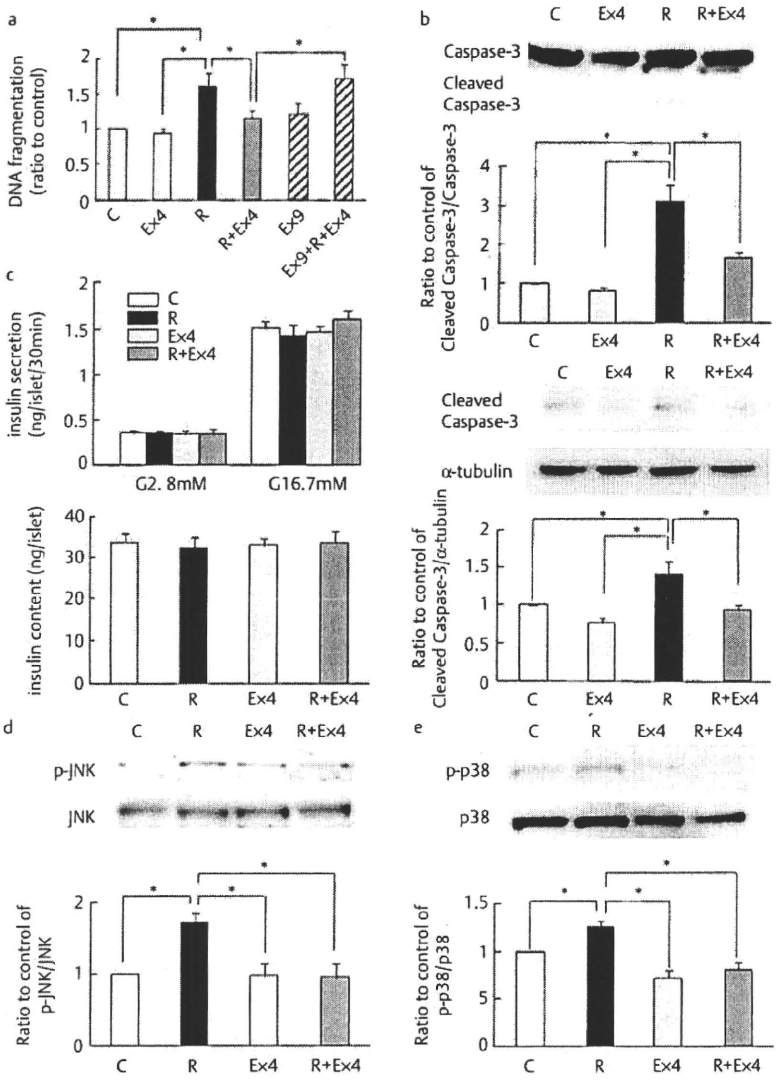

Fig. 4 Exendin-4 inhibits cell death and phosphorylation of JNK and p38 induced by rapamycin in Wistar rat primary islets. **a**: Primary islets were treated with 10 nM rapamycin and/or 10 nM exendin-4 and/or 100 nM exendin-9 for 12 h, and dead cells were detected by DNA fragmentation. Data are means ± SE of three independent experiments. * $p < 0.05$ **b**: Western blot analysis of caspase-3 and cleaved caspase-3 in primary islets treated with 10 nM rapamycin and/or 10 nM exendin-4 for 12 h. Images are representative of three independent experiments. Graphs show relative ratio of cleaved caspase-3 v.s. caspase-3 or α-tubulin, respectively. * $p < 0.05$. **c**: Glucose-stimulated insulin secretion and insulin content in Wistar rat islets treated with 10 nM rapamycin and/or 10 nM exendin-4 for 12 h. Data are means ± SE of three independent experiments. **d, e**: Primary islets were treated with 10 nM rapamycin and/or 10 nM exendin-4 for 30 min, and phosphorylation of JNK and p38 was detected by western blot. Images are representative of three independent experiments. Graphs show relative ratio of phosphorylated JNK or p38 vs. total JNK or p38, respectively, by treatment with rapamycin and/or exendin-4 compared to control (DMSO). Data are means ± SE of four independent experiments. * $p < 0.05$. C: control (DMSO); R: rapamycin; Ex4: exendin-4; Ex9: exendin-9; G: glucose.

Exendin-4 inhibits phosphorylation of JNK and p38 induced by rapamycin

To confirm the involvement of JNK and p38 in rapamycin-induced cell death, MIN6 cells were incubated with 10 nM rapamycin for 30 min, and phosphorylation of JNK and p38 was detected by western blot analysis. Phosphorylation of JNK and p38 was significantly increased 2.9 ± 0.2-fold and 1.6 ± 0.3-fold, respectively, compared to that in nontreated cells (○ **Fig. 3b** and **c**). In contrast, 10 nM exendin-4 decreased phosphorylation of both JNK and p38 in rapamycin-treated MIN6 cells (○ **Fig. 3b** and **c**). However, rapamycin and exendin-4 were found not to affect phosphorylation of mitogen-activated protein kinase kinase (MKK) 3/6, a kinase of p38, or MKK4, a kinase of JNK (data not shown), indicating that dephosphorylation of both JNK and p38 by exendin-4 is not mediated by these upstream kinases.

PKA is involved in dephosphorylation of p38 by exendin-4

Because PKA partially inhibited rapamycin-induced cell death, we examined the effect of H89 on JNK and p38 phosphorylation. Fifteen μM H89 was added into the media of MIN6 cells 30 min before treatment with 10 nM rapamycin and/or 10 nM exendin-4 for 30 min, when phosphorylation of JNK and p38 was detected by western blot analysis. H89 did not affect decreased phosphorylation of JNK by exendin-4 (○ **Fig. 3d**). By contrast, H89 significantly inhibited dephosphorylation of p38 by exendin-4 (○ **Fig. 3e**), indicating that PKA regulates p38 phosphorylation.

Exendin-4 inhibits rapamycin-induced cell death and phosphorylation of JNK and p38 in Wistar rat islets

We lastly investigated whether exendin-4 inhibits cell death induced by rapamycin in primary islets by affecting phosphorylation of JNK or p38. Wistar rat islets were treated with 10 nM rapamycin and/or 10 nM exendin-4 for 12 h, and the number of dead cells was determined by DNA fragmentation. Rapamycin significantly increased DNA fragmentation by 1.6 ± 0.2-fold compared to that of control (DMSO) (○ **Fig. 4a**), while exendin-4 significantly inhibited rapamycin-induced DNA fragmentation (○ **Fig. 4a**). Exendin-9 again completely blocked the cytoprotective effect of exendin-4 (○ **Fig. 4a**), indicating that such cytoprotective effect of exendin-4 is mediated by the GLP-1 receptor in primary islets. Caspase-3 activity also was significantly increased in rapamycin-treated islets, which was prevented by treatment with exendin-4 (○ **Fig. 4b**). To determine whether the surviving

cells treated with exendin-4 were actually beta cells, islet beta cells were stained with Newport Green, a fluorescent indicator of zinc that allowed visualization of islet beta cells [17] after treatment with 10 nM rapamycin and/or 10 nM exendin-4 for 12 h. Fluorescence microscopy revealed Newport Green positive cells treated with rapamycin and exendin-4 that are almost the same as those treated with DMSO (control) or exendin-4 alone (data not shown). In addition, insulin content and glucose-stimulated insulin secretion (GSIS) were compared among rapamycin- and/or exendin-4-treated Wistar rat islets to determine whether or not these islets are still functional. After islets were incubated with 10 nM rapamycin and/or 10 nM exendin-4 for 12 h, the rapamycin and exendin-4 were washed out and the islets were then stimulated with 2.8 mM or 16.7 mM glucose for 30 min. The amounts of GSIS and insulin content were almost the same in rapamycin- and exendin-4-treated islets, indicating that islets treated with rapamycin and exendin-4 for 12 h are still functional (○ **Fig. 4c**).

Finally, regulation of JNK and p38 by rapamycin or exendin-4 in primary islets was examined. Incubation with 10 nM rapamycin for 30 min significantly increased phosphorylation of JNK and p38 by 1.7±0.2-fold and 1.3±0.1-fold, respectively, which was reversed to control level by coincubation with exendin-4 (○ **Fig. 4d** and **e**). These results indicate that exendin-4 protects primary islets from rapamycin-induced cytotoxicity by decreasing phosphorylation of JNK and p38.

Discussion

In the present study, we have demonstrated that rapamycin induces cytotoxicity in MIN6 cells and Wistar rat islets by phosphorylating JNK and p38, and that exendin-4 inhibits this effect by inhibiting phosphorylation of JNK and p38. This is the first report indicating that rapamycin and exendin-4 regulate phosphorylation not only of JNK but also of p38 in primary islets.

The molecular mechanism of the cytoprotective effect of exendin-4 is mediated by increased levels of cAMP that lead to activation of PKA, enhanced IRS-2 activity, and activation of Akt and ERK [7]. Our data also reveal that an increase in the cAMP concentration completely blocked rapamycin-induced cell death. However, LY294002 and PD98059 did not affect rapamycin-induced beta cell death, even though exendin-4 increased Akt and ERK phosphorylation. Phosphorylation of Akt and ERK also were not affected by treatment with rapamycin, suggesting that these kinases are not directly involved in the cytoprotective effect of exendin-4 on rapamycin-induced beta cell death.

On the other hand, exendin-4 and rapamycin both regulate phosphorylation of JNK and p38 in islet beta cells. Rapamycin increases JNK and p38 phosphorylation; exendin-4 decreases their phosphorylation. JNK and p38 are activated by cellular stress, and lead the cells to apoptosis [18]. In islet beta cells, phosphorylation of JNK and p38 are involved in cell death induced by IL-1β [19,20] and islet isolation [21,22]. Conversely, inhibition of JNK or p38 with specific inhibitors prevents cell death induced by islet isolation [22,23], indicating that JNK and p38 are significant molecules in pancreatic beta cell death. In addition, when Wistar rat islets were preincubated for 24 h, rapamycin decreased GSIS, most likely due to reduction in mitochondrial ATP production in the islets of these rats [24]. JNK and p38 are involved in beta-cell function, their activation also affecting insulin biosynthesis. JNK activates c-Jun, a downstream protein, and inhibits insulin gene transcription [25]. Furthermore, the p38 molecule is reported to repress rat insulin gene 1 promoter activated by GLP-1 [26]. Although insulin secretion and insulin content were not affected by pretreatment with 10 nM rapamycin and/or 10 nM exendin-4 for 12 h, inhibition of JNK and p38 activity by treatment with exendin-4 for a longer time may not only inhibit beta cell apoptosis but also increase insulin biosynthesis.

In summary, exendin-4 can inhibit rapamycin-induced beta cell death via a decrease in phosphorylation of both JNK and p38, and dephosphorylation of p38 by exendin-4 is accomplished at least partially through PKA signaling pathways. These results demonstrate that regulation of both JNK and p38 is important in the cytoprotective action of exendin-4 against rapamycin in pancreatic beta cells.

Acknowledgements

This study was supported by Scientific Research Grants from the Ministry of Education, Culture, Sports, Science, and Technology, Japan, and from the Ministry of Health, Labor, and Welfare, Japan, and also by Kyoto University Global COE Program "Center for Frontier Medicine".

Affiliations

[1] Department of Diabetes and Clinical Nutrition, Graduate School of Medicine, Kyoto University, Kyoto, Japan
[2] Japan Association for the Advancement of Medical Equipment, Tokyo, Japan
[3] Department of Endocrinology and Diabetes and Geriatric Medicine, Akita University School of Medicine, Akita, Japan
[4] Kansai Electric Power Hospital, Osaka, Japan
[5] CREST of Japan Science and Technology Cooperation (JST), Kyoto, Japan

References

1 *Kendall DM, Riddle MC, Rosenstock J, Zhuang D, Kim DD, Fineman MS, Baron AD.* Effects of exenatide (exendin-4) on glycemic control over 30 weeks in patients with type 2 diabetes treated with metformin and a sulfonylurea. Diabetes Care 2005; 28: 1083–1091
2 *Baggio LL, Drucker DJ.* Biology of incretins: GLP-1 and GIP. Gastroenterology 2007; 132: 2131–2157
3 *Li L, El-Kholy W, Rhodes CJ, Brubaker PL.* Glucagon-like peptide-1 protects beta cells from cytokine-induced apoptosis and necrosis: role of protein kinase B. Diabetologia 2005; 48: 1339–1349
4 *Yusta B, Baggio LL, Estall JL, Koehler JA, Holland DP, Li H, Pipeleers D, Ling Z, Drucker DJ.* GLP-1 receptor activation improves beta cell function and survival following induction of endoplasmic reticulum stress. Cell Metab 2006; 4: 391–406
5 *Wang Q, Brubaker PL.* Glucagon-like peptide-1 treatment delays the onset of diabetes in 8 week-old db/db mice. Diabetologia 2002; 45: 1263–1273
6 *Li Y, Hansotia T, Yusta B, Ris F, Halban PA, Drucker DJ.* Glucagon-like peptide-1 receptor signaling modulates beta cell apoptosis. J Biol Chem 2003; 278: 471–478
7 *Brubaker PL, Drucker DJ.* Minireview: Glucagon-like peptides regulate cell proliferation and apoptosis in the pancreas, gut, and central nervous system. Endocrinology 2004; 145: 2653–2659
8 *Tews D, Lehr S, Hartwig S, Osmers A, Paslack W, Eckel J.* Anti-apoptotic action of exendin-4 in INS-1 beta cells: comparative protein pattern analysis of isolated mitochondria. Horm Metab Res 2009; 41: 294–301
9 *Bell E, Cao X, Moibi JA, Greene SR, Young R, Trucco M, Gao Z, Matschinsky FM, Deng S, Markman JF, Naji A, Wolf BA.* Rapamycin has a deleterious effect on MIN-6 cells and rat and human islets. Diabetes 2003; 52: 2731–2739
10 *Fraenkel M, Ketzinel-Gilad M, Ariav Y, Pappo O, Karaca M, Castel J, Berthault MF, Magnan C, Cerasi E, Kaiser N, Leibowitz G.* mTOR inhibition by rapamycin prevents beta-cell adaptation to hyperglycemia and exacerbates the metabolic state in type 2 diabetes. Diabetes 2008; 57: 945–957

11 *Fujimoto S, Ishida H, Kato S, Okamoto Y, Tsuji K, Mizuno N, Ueda S, Mukai E, Seino Y.* The novel insulinotropic mechanism of pimobendan: Direct enhancement of the exocytotic process of insulin secretory granules by increased Ca2+ sensitivity in beta-cells. Endocrinology 1998; 139: 1133–1140

12 *Leist M, Gantner F, Bohlinger I, Germann PG, Tiegs G, Wendel A.* Murine hepatocyte apoptosis induced in vitro and in vivo by TNF-alpha requires transcriptional arrest. J Immunol 1994; 153: 1778–1788

13 *Webster AC, Lee VW, Chapman JR, Craig JC.* Target of rapamycin inhibitors (sirolimus and everolimus) for primary immunosuppression of kidney transplant recipients: a systematic review and meta-analysis of randomized trials. Transplantation 2006; 81: 1234–1248

14 *Huang S, Shu L, Dilling MB, Easton J, Harwood FC, Ichijo H, Houghton PJ.* Sustained activation of the JNK cascade and rapamycin-induced apoptosis are suppressed by p53/p21(Cip1). Mol Cell 2003; 11: 1491–1501

15 *Bachar E, Ariav Y, Ketzinel-Gilad M, Cerasi E, Kaiser N, Leibowitz G.* Glucose amplifies fatty acid-induced endoplasmic reticulum stress in pancreatic beta-cells via activation of mTORC1. PLoS One 2009; 4: e4954

16 *Rincón M, Davis RJ.* Regulation of the immune response by stress-activated protein kinases. Immunol Rev 2009; 228: 212–224

17 *Lukowiak B, Vandewalle B, Riachy R, Kerr-Conte J, Gmyr V, Belaich S, Lefebvre J, Pattou F.* Identification and purification of functional human beta-cells by a new specific zinc-fluorescent probe. J Histochem Cytochem 2001; 49: 519–528

18 *Mandrup-Poulsen T.* beta-cell apoptosis: stimuli and signaling. Diabetes 2001; 50 (Suppl 1): S58–S63

19 *Ammendrup A, Maillard A, Nielsen K, Aabenhus Andersen N, Serup P, Dragsbaek Madsen O, Mandrup-Poulsen T, Bonny C.* The c-Jun amino-terminal kinase pathway is preferentially activated by interleukin-1 and controls apoptosis in differentiating pancreatic beta-cells. Diabetes 2000; 49: 1468–1476

20 *Saldeen J, Lee JC, Welsh N.* Role of p38 mitogen-activated protein kinase (p38 MAPK) in cytokine-induced rat islet cell apoptosis. Biochem Pharmacol 2001; 61: 1561–1569

21 *Abdelli S, Ansite J, Roduit R, Borsello T, Matsumoto I, Sawada T, Allaman-Pillet N, Henry H, Beckmann JS, Hering BJ, Bonny C.* Intracellular stress signaling pathways activated during human islet preparation and following acute cytokine exposure. Diabetes 2004; 53: 2815–2823

22 *Ito T, Omori K, Rawson J, Todorov I, Asari S, Kuroda A, Shintaku J, Itakura S, Ferreri K, Kandeel F, Mullen Y.* Improvement of canine islet yield by donor pancreas infusion with a p38MAPK inhibitor. Transplantation 2008; 86: 321–329

23 *Noguchi H, Nakai Y, Matsumoto S, Kawaguchi M, Ueda M, Okitsu T, Iwanaga Y, Yonekawa Y, Nagata H, Minami K, Masui Y, Futaki S, Tanaka K.* Cell permeable peptide of JNK inhibitor prevents islet apoptosis immediately after isolation and improves islet graft function. Am J Transplant 2005; 5: 1848–1855

24 *Shimodahira M, Fujimoto S, Mukai E, Nakamura Y, Nishi Y, Sasaki M, Sato Y, Sato H, Hosokawa M, Nagashima K, Seino Y, Inagaki N.* Rapamycin impairs metabolism-secretion coupling in rat pancreatic islets by suppressing carbohydrate metabolism. J Endocrinol 2010; 204: 37–46

25 *Inagaki N, Maekawa T, Sudo T, Ishii S, Seino Y, Imura H.* c-Jun represses the human insulin promoter activity that depends on multiple cAMP response elements. Proc Natl Acad Sci USA 1992; 89: 1045–1049

26 *Kemp DM, Habener JF.* Insulinotropic hormone glucagon-like peptide 1 (GLP-1) activation of insulin gene promoter inhibited by p38 mitogen-activated protein kinase. Endocrinology 2001; 142: 1179–1187

Original Paper

Neonatology
formerly Biology of the Neonate

Neonatology 2010;98:179–190
DOI: 10.1159/000283994

Received: June 30, 2009
Accepted after revision: December 10, 2009
Published online: March 16, 2010

Assessment of a New Piezoelectric Transducer Sensor for Noninvasive Cardiorespiratory Monitoring of Newborn Infants in the NICU

Shinichi Sato[a] Wako Ishida-Nakajima[b] Akira Ishida[b] Masanari Kawamura[b] Shinobu Miura[b] Kyoichi Ono[a] Nobuya Inagaki[c, d] Goro Takada[b] Tsutomu Takahashi[b]

Departments of [a]Cell Physiology and [b]Pediatrics, Akita University Graduate School of Medicine, Akita, [c]Department of Diabetes and Clinical Nutrition, Kyoto University Graduate School of Medicine, Kyoto, and [d]CREST of Japan Science and Technology Agency, Kawaguchi, Japan

Key Words

Cardiorespiratory monitoring, noninvasive · Piezoelectric transducer sensor · Heart sounds · Breathing movement · Motion artifact · Electrocardiogram · Impedance pneumography · Skin damage

Abstract

Background: Electrocardiogram (ECG) and impedance pneumography (IPG), the most widely used techniques for cardiorespiratory monitoring in the neonatal intensive care unit (NICU), have the disadvantage of causing skin damage when used for very premature newborn infants. To prevent skin damage, we designed a new piezoelectric transducer (PZT) sensor. ***Objective:*** To assess the potential of the PZT sensor for cardiorespiratory monitoring in the NICU. ***Methods:*** The PZT sensor was placed under a folded towel under a neonate to detect an acoustic cardiorespiratory signal, from which heart rate (HR) and breathing rate (BR) were calculated, together with simultaneous ECG/IPG recording for 1–9 days for long and brief (1-min) assessment. ***Results:*** The brief assessment showed average correlation coefficients of 0.92 ± 0.12 and 0.95 ± 0.02 between instantaneous HRs/BRs detected by the PZT sensor and ECG/IPG in 27 and 11 neonates examined. During the long assessment, the HR detection rate by the PZT sensor was ~10% lower than that by ECG (82.6 ± 12.9 vs. 91.8 ± 4.1%; $p = 0.001$, $n = 27$), although comparable (90.3 ± 4.1 vs. 92.5 ± 3.4%, $p = 0.081$) in ~70% (18/27) of neonates examined; BR detection rate was comparable between the PZT sensor and IPG during relatively stable signal conditions (95.9 ± 4.0 vs. 95.3 ± 3.5%; $p = 0.38$, $n = 11$). The PZT sensor caused neither skin damage nor body movement increase in all neonates examined. ***Conclusion:*** The PZT sensor is noninvasive and does not cause skin irritation, and we believe it does provide a reliable, accurate cardiorespiratory monitoring tool for use in the NICU, although the issue of mechanical-ventilation noise remains to be solved.

Copyright © 2010 S. Karger AG, Basel

Introduction

Cardiorespiratory monitoring of infants in the neonatal intensive care unit (NICU) is generally performed by electrocardiogram (ECG) and respiratory impedance pneumography (IPG), which utilizes ECG electrodes. These techniques are robust and widely used in the NICU

KARGER

Fax +41 61 306 12 34
E-Mail karger@karger.ch
www.karger.com

© 2010 S. Karger AG, Basel
1661–7800/10/0982–0179$26.00/0

Accessible online at:
www.karger.com/neo

Shinichi Sato, PhD
Department of Cell Physiology, Akita University Graduate School of Medicine
1-1-1 Hondo
010-8543 Akita (Japan)
Tel. +81 18 884 6070, Fax +81 18 836 2604, E-Mail bigwave@gipc.akita-u.ac.jp

although the attachment of adhesive ECG electrodes is often difficult and is responsible for skin damage when it is used for very premature newborn infants or neonates after surgery [1]. In the pursuit of completely noninvasive cardiorespiratory monitoring, it is desirable for electrodes and sensors not to come into contact with the skin of a neonate. To solve this problem, other methods have been proposed to prevent skin damage at the site of ECG electrode attachment: a synthetic skin covering to protect the skin of low birth weight infants [1], a shirt incorporating a cardiorespiratory monitor [2] and a respiratory inductive plethysmography system that utilizes a belt-type sensor that requires passing no current through the neonate's body [3]. An electronic stethoscope [4] and echocardiography [5, 6] are also advanced methods which use no ECG electrodes to examine cardiac function, but their sensors still need to be in contact with the skin of a neonate and are unlikely to be suitable for cardiac monitoring over a long period. Recently, we developed a noninvasive cardiorespiratory-monitoring system for mice using a piezoelectric transducer (PZT) sensor (ATC-402; Unique Medical, Japan) [7–9], and based on this, we designed a PZT sensor for newborn infants (Pat. pending: PCT/JP2005/012068). As the PZT sensor is covered with a folded towel under the neonate, it never comes into contact with the skin (fig. 1). The PZT sensor passively detects acoustic vibrations produced by the heartbeats and breathing movements of a neonate and converts them into an electrical signal, from which the heart rate (HR) and breathing rate (BR) can be calculated. In the present study, we assessed the performance and feasibility of the new noninvasive PZT sensor for cardiorespiratory monitoring of newborn infants in the NICU by comparing with ECG and IPG.

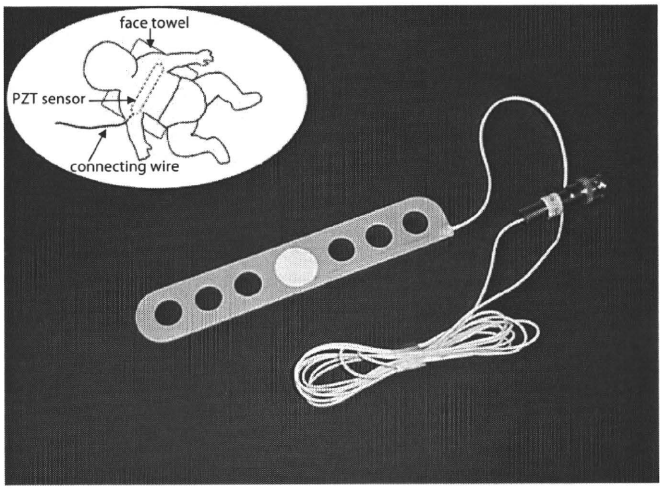

Fig. 1. PZT sensor. A round and thin PZT adheres to the lower side and center of a flexible plastic plate (width × depth × height, 180 × 30 × 1 mm) with several holes. The PZT sensor is put under a folded towel (~5 mm thick), on which a neonate is placed for cardiorespiratory monitoring, as illustrated in the inset. The PZT sensor was approved by the Ministry of Health, Labour and Welfare in Japan (No. 13B1X10014).

Methods

Subjects

Ethics approval for this project was granted by the Human Ethics Committee of Akita University School of Medicine. Seventy-nine neonates (50 boys and 29 girls) born at 25–42 (median 35) weeks of gestational age (GA) with birth weights (BWs) of 742–4,126 (median 2,140) g were recruited from the NICU, Akita University Hospital (table 1). Cardiorespiratory monitoring by PZT sensor was performed from June 2004 to January 2008 in 69 neonates, whose parents received oral information about the purpose of the study and gave written consent. Another 10 neonates underwent conventional ECG monitoring without the PZT sensor to assess if there is an adverse effect of the PZT sensor on neonates. Although 298 inpatients were eligible, only a small population was enrolled in the study because we had only one or two PZT sensor systems available for measurement during the period.

We carefully performed a preliminary study for 2 years from 2004 with 25 neonates to confirm the practical use of a PZT sensor for cardiorespiratory monitoring in the NICU and to determine the shape of the PZT sensor. Connections to a patient monitor to record ECG and IPG became available in June 2006 and May 2007, respectively. After the preliminary study and approval of the PZT sensor by the Ministry of Health, Labour and Welfare in Japan (approval No. 13B1X10014), we performed HR and BR measurements using the approved PZT sensor in 29 (from 2006) and 15 (from 2007) neonates, respectively, to evaluate the PZT sensor system. Six data were omitted from analysis: 2 poor quality data of unknown causes and 4 data obtained with misconnections to the A/D converter in HR and BR measurement, respectively. Finally, a total of 63 data (25 + 27 + 11) were used for the assessment of the PZT sensor.

PZT Sensor Construction

The preliminary study led to the conclusion that the PZT sensor should be as small as possible for a neonate to sleep comfortably with no accompanying irritation or discomfort; therefore, we designed a PZT sensor that consisted of a thin PZT (EE27A-39A; FDK, Japan) and flexible plastic plate (width × depth × height, 180 × 30 × 1 mm) with several holes, in the middle of which the PZT was adhered (fig. 1). The holes in the plastic plate may help to prevent skin damage (bedsores), enabling air ventilation and diffusing moisture produced by sweat through the towel (~5 mm thick) placed between the neonate and the PZT sensor. The plastic plate was designed to collect the vibrations of heartbeats and breathing movements from a wide area and therefore the PZT sensor allows slight displacement from the best monitoring position.

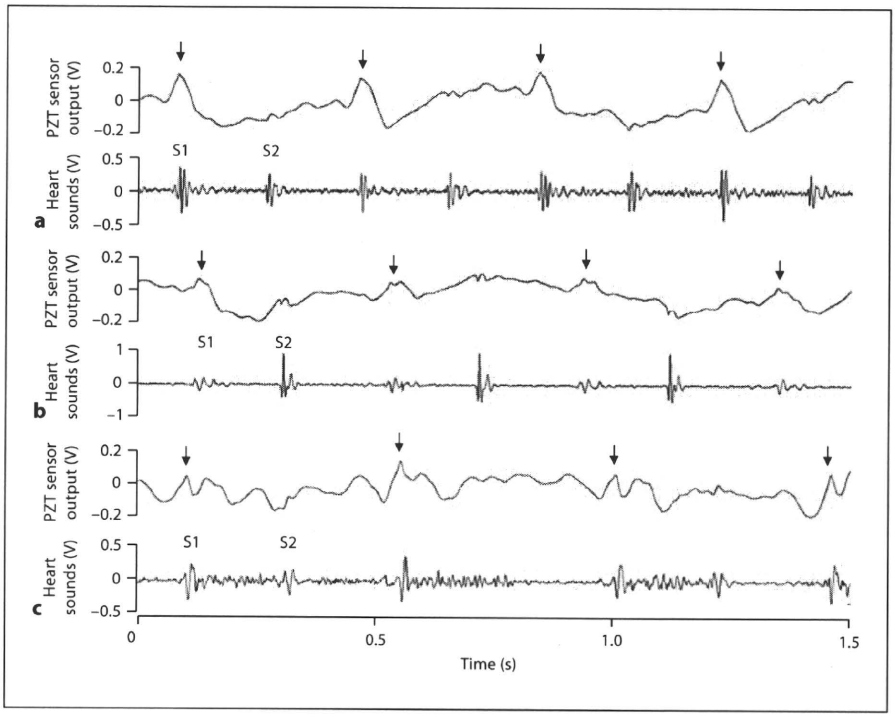

Fig. 2. PZT sensor output (upper) and filtered and amplified heart sounds (lower) with normal shape (**a**), accentuated second sounds (**b**) and heart murmurs (**c**) recorded in the preliminary study. Low frequency components of S_1 (arrows) were detected in the PZT sensor outputs, which are likely to indicate gross heart movement and have different waveforms between the three traces.

Data Recording

The PZT sensor was fixed with an adhesive plaster to a towel-covered foam mattress in an incubator and covered with a folded face towel, on which the neonate was placed; therefore, there were 2 layers of towel cloth between the PZT sensor and the back (or chest/abdomen) of the neonate (fig. 1). Adhesive ECG electrodes were also attached to the chest or back of a neonate for ECG/IPG. In addition, other catheters, tubes or sensors (orogastric tube, percutaneous central venous catheter, oxygen saturation monitor) were used for all neonates, while an orotracheal tube, transcutaneous CO_2 monitor and umbilical arterial/venous catheter were additionally used for serious cases. After placing the PZT sensor under a neonate, a physician or nurse corrected the neonate's position as usual during their routine work, but no attention was paid to the PZT sensor setting during the measurement. In addition, the sleeping position of all neonates was routinely changed at every 3 h into either supine, prone, right or left (side down) lateral position.

PZT sensor output and ECG signal output from a patient monitor (DS-5100E; Fukuda Denshi, Japan) were uploaded to a computer installed with data acquisition software (Axoscope9; Molecular Devices, USA) via a 2-channel A/D converter. Another data recording system (Acquisition 2.0; Unique Medical) was used for three-channel recording including respiratory signal of IPG in addition to the above signals. Heart sounds, breathing movement signals and other digital outputs of the PZT system were not recorded so as to maintain data less than ~1 Gbyte; data were sampled at 2-millisecond intervals to give a maximum file size for continuous recordings over 3 days of ~1 Gbyte. Measurement for each neonate was started at 0 (median, range 0–8) days and continued for 1–9 days. In the preliminary study, PZT sensor output and ECG signal were recorded for 5–10 min by a data recorder (PC204Ax; Sony, Japan) at a sampling rate of 20 kHz to analyze the heart sound waveform (fig. 2).

Brief Assessment of Inherent Performance of the PZT Sensor

Inherent performance of the PZT sensor was assessed using data analysis software (Clampfit 9.2; Molecular Devices), which is often used to analyze the firing rate of spontaneously firing cells, and a spreadsheet application (Excel; Microsoft, USA) after data recording. Firstly, the PZT sensor output signal was filtered (high-pass 70 Hz: 8-pole Bessel) by a filter of the data analysis software to extract heart sounds. Secondly, heart sounds and ECG signals for 1 min each were extracted from periods when no large noise, fluctuation, arrhythmia and apnea occurred. Thirdly, the peak time data of every first sound (S_1) and second sound (S_2) in the heart sound signal were then automatically sampled by template search analysis (a type of pattern recognition processing) of the data analysis software, which searches the whole record for similar signals with a predefined representative S_1 epoch regardless of their amplitude. Then, using the spreadsheet application, S_1–S_1 intervals were compared with corresponding R–R intervals, which were similarly obtained from the ECG by template search analysis after a filtering process (high-pass >5 Hz). S_1–S_1 interval errors arising from multi-peaks of the S_1 signal [7] were manually corrected. Twenty-seven neonates (19 boys and 8 girls; GA 34.5 ± 3.5 weeks, BW 2,027 ± 800 g) were recruited for this assessment (table 1). Similarly, respiration signals obtained by the PZT sensor and IPG for 1 min each were extracted and band-pass filtered (0.5–0.6 and 0.5–0.8 Hz, respectively) to obtain the breathing intervals of 11 newborn infants (5 boys and 6 girls; GA 35.0 ± 3.6

Table 1. Clinical characteristics of patients enrolled in long and short period assessments of heart rate and breathing rate detection by the PZT sensor and those in body motility assessment in 2 groups that underwent ECG recording with and without the PZT sensor measurement

	Long and short period assessments		Body motility assessment	
	heart rate (n = 27)	breathing rate (n = 11)	ECG + PZT sensor (n =10)	ECG only (n = 10)
Age at measurement, days	0 [0–3]	1 [0–5]	1 [0–5]	0 [0–3]
Gestational age at birth, weeks	34.9 [25.3–39.9]	35.0 [28.6–41.1]	34.0 [28.6–40.7]	35.2 [32.3–40]
Boys	19 (70)	5 (45)	5 (50)	6 (60)
Neonatal weight, g	1,960 [742–4,126]	2,157 [1,117–3,316]	2,152 [1,117–2,852]	2,029 [1,302–2,434]
ELBW	2 (7.4)	0 (0)	0 (0)	0 (0)
VLBW	5 (18.5)	2 (18.2)	2 (20)	2 (20)
LBW	14 (51.9)	6 (54.5)	6 (60)	8 (80)
Diagnosis				
Amniotic infection	1 (3.7)	0 (0)	0 (0)	0 (0)
Anal atresia	1 (3.7)	0 (0)	0 (0)	0 (0)
Asphyxia	1 (3.7)	0 (0)	0 (0)	0 (0)
Asphyxia neonatorum	1 (3.7)	0 (0)	0 (0)	0 (0)
Atrial septal defect	1 (3.7)	0 (0)	0 (0)	0 (0)
Chromosome abnormality	1 (3.7)	0 (0)	0 (0)	0 (0)
Cleft of the soft palate	0 (0)	1 (9.1)	0 (0)	0 (0)
Down syndrome	2 (7.4)	0 (0)	0 (0)	0 (0)
Duodenal atresia	1 (3.7)	0 (0)	0 (0)	0 (0)
Patent ductus arteriosus	2 (7.4)	1 (9.1)	1 (10)	0 (0)
Patent foramen ovale	1 (3.7)	0 (0)	0 (0)	0 (0)
Peripheral pulmonary stenosis	1 (3.7)	0 (0)	0 (0)	0 (0)
Pierre Robin sequence	0 (0)	1 (3.7)	0 (0)	0 (0)
Pneumothorax	1 (3.7)	0 (0)	0 (0)	0 (0)
Respiratory distress syndrome	3 (11.1)	0 (0)	0 (0)	0 (0)
Transient tachypnea of the newborn	2 (7.4)	1 (9.1)	1 (10)	0 (0)
Transient myeloproliferative disease	2 (7.4)	0 (0)	0 (0)	0 (0)
Ventriculomegaly	0 (0)	1 (9.1)	1 (10)	0 (0)
Mechanical ventilation				
Nasal continuous positive airway pressure	3 (11.1)	0 (0)	0 (0)	0 (0)
Intermittent mandatory ventilation	2 (7.4)	0 (0)	0 (0)	0 (0)
High frequency oscillation	2 (7.4)	1 (9.1)	1 (10)	0 (0)

Data are expressed as medians with ranges in square brackets or numbers with percentages in parentheses.

weeks, BW 2,150 ± 650 g) by template search analysis to compare the breathing interval between the two methods. These comparisons of cardiac and breathing intervals during a short period were finally evaluated by the correlation coefficient and Bland-Altman plot using a spreadsheet application.

Assessment of PZT Sensor Measurement of a Long Duration

Long-term assessment was unavoidably simplified because the manual verification/correction of 1-min PZT data took 2 h and a 1-week data set would take ~10 years. However, the manual verification of data was not completely abandoned but we verified data as much as possible, searching for errors by observing HR/BR trend graphs and reanalyzing the periods with vertical lines (fig. 3), which indicate false positives/negatives or noises, by changing threshold and template for template search analysis or by measuring signal peaks manually.

Detection rates of HR and BR during >10 h (9 days maximum) long measurement by the PZT system and ECG/IPG were evaluated according to the total time during which cardiac beats and respiratory activity were identified by template search analysis. For the evaluation, raw data were divided into 24-hour records. The divided data were then subjected to template search analysis to obtain a series of S_1 and S_2 time peaks and peaks of R waves after high-pass filtering of 70 and 5 Hz, respectively. These peak time data were used to calculate instantaneous HR using a spreadsheet application; HRs between 100 and 380 (beats/min) were scored as correct because detecting the S_1–S_2 or S_2–S_1 interval doubled the HR (fig. 3a, upper), while an acceptable cardiac inter-

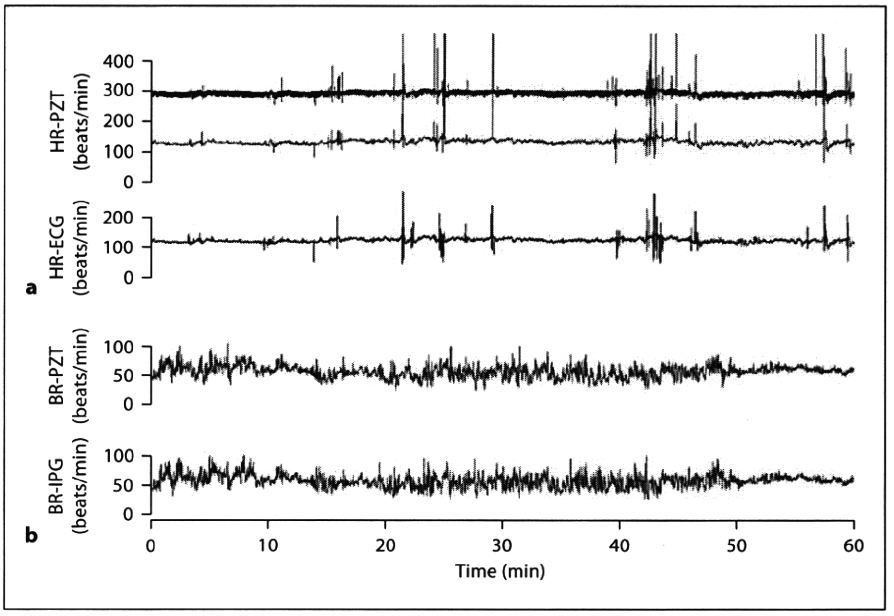

Fig. 3. Time courses of HR and BR for 1 h measured by the PZT sensor system and ECG/IPG. **a** Instantaneous HR detected by the PZT sensor system (HR-PZT: upper) and that by ECG (HR-ECG: lower). HR-PZT has 2 traces: the upper trace indicates doubled HR calculated from S_1–S_2 and S_2–S_1 intervals; the lower trace indicates HR calculated from S_1–S_1 [= (S_1–S_2) + (S_2–S_1)] intervals. HRs detected by the PZT sensor and ECG were in good agreement. Several vertical lines indicate false positives/negatives or detection errors caused by noises. **b** BR averaged every two consecutive BRs detected by the PZT sensor system (BR-PZT: upper) and that by IPG (BR-IPG: lower), which were in good agreement.

val surrounded by several abnormal intervals (i.e., noisy condition) was scored as a failure to avoid overestimation. This automatic analysis method seems to be reliable because a HR detection rate of 95.7% during 10,000 s of representative data, including signal artifacts in part, was only 0.4% lower than that after a thorough manual correction. In ECG analysis, an HR between 100 and 200 beats/min was scored as correct. Finally, the HR detection rate, i.e., % time of successful cardiac cycle detection to total recording time, was calculated and compared between the PZT sensor and ECG measurements.

Similarly, the BR detection rate between the PZT sensor and IPG was compared by template search analysis and a spreadsheet application after band-pass filtering of 0.5–0.6 and 0.5–0.8 Hz, respectively. These comparisons were performed on selected data area with fewer motion artifacts, which were distinguished by analyzing template search analysis data; e.g., peak amplitude, maximum rise slope, instantaneous frequency, change in peak-peak interval and change in peak amplitude.

As the evaluations of false positive and negative in bradycardia and apnea are difficult in the case when ECG/IPG missed signals although the PZT signal was good, and because of huge data size, only false negatives in bradycardia/apnea detection were evaluated during the period when ECG/IPG detected bradycardia/apnea. Bradycardias of <80 beats/min for >5 s and apneas of >15 s in 27 and 11 neonates, respectively, were compared between the PZT sensor system and ECG/IPG.

Assessment of Discomfort

To assess whether the PZT sensor under the body is uncomfortable for a neonate, we compared the total amount of body movements of neonates with and without the PZT sensor. A cluster of body movements was counted when the baseline deflection of raw IPG signal exceeded ±2 V and it was repeated at intervals of <20 s, and the time between the first and last deflection was determined as the duration of body movement. The total time of body movements, including brief movements (twitch), was summed over the period of measurement in each neonate using a spreadsheet application. Ten newborn infants (5 boys and 5 girls; 2 VLBW and 8 LBW; median GA = 35.2 weeks; median BW = 2,029 g), with no complications were subjected to ECG measurement without the PZT sensor to compare with the data of 10 neonates (6 boys and 4 girls; 2 VLBW, 6 LBW and 2 normal weight; GA = 34.0 weeks; BW = 2,152 g) who underwent ECG with the PZT sensor recording (table 1). For the latter 10 neonates, 2/27 and 8/11 subjects were chosen from among the neonates who underwent the HR and BR (brief/long) assessment, respectively. No significant difference was found in GA ($p = 0.31$), weight ($p = 0.83$) and Apgar score ($p = 0.11$; 9 vs. 10, at 5 min, median) between the 2 groups with and without the PZT sensor recording.

Statistical Analysis

Statistical significance between groups was assessed depending on the homogeneity of variance by Student's t test or Welch's t test. Wilcoxon's non-parametric test was also applied to reveal significant differences. Data are expressed as the mean ± SD, and $p < 0.05$ was considered significant. Mann-Whitney's U test was used for the comparison of Apgar scores.

Results

We successfully detected heart sounds and breathing movements of newborn infants in the preliminary study using our custom-designed PZT sensor and an electric circuit similar to the cardiorespiratory monitor for mice (fig. 2) [7–9]. Differences in the signal waveform of heart

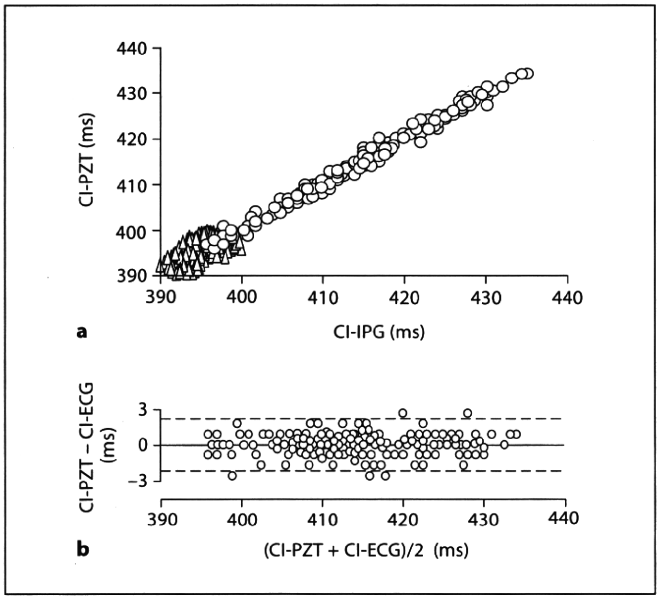

Fig. 4. Results of brief analysis of cardiac interval detection. Representative cross-correlation (**a**; open circles, r = 0.99) and difference plots (**b**) between the cardiac interval (CI) detected by PZT sensor (CI-PZT) and that by ECG (CI-ECG). Solid and broken lines indicate the means ± 2 SD. Superimposed open-triangle plots (**a**; r = 0.67) aggregated below the interval of 400 ms depict reduced heart rate variability of 1 ELBW patient.

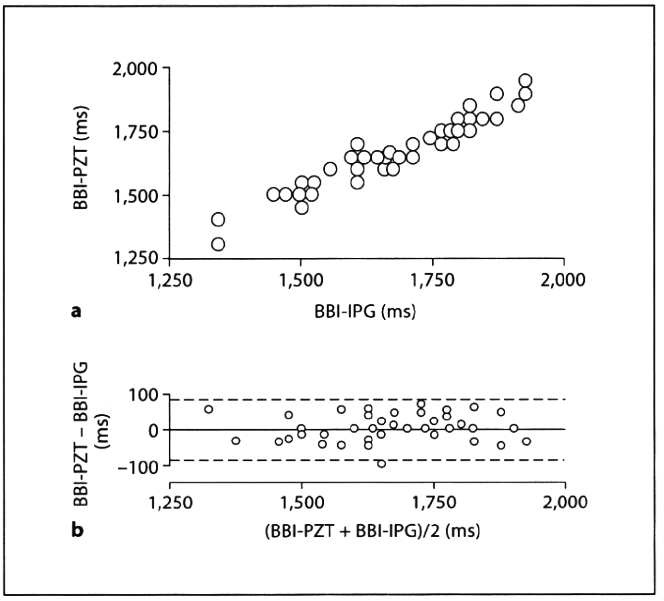

Fig. 5. Result in brief analysis of breathing interval detection. Representative cross-correlation (**a**; open circles, r = 0.96) and difference plots (**b**) between the breath-to-breath interval (BBI) detected by PZT sensor (BBI-PZT) and that by IPG (BBI-IPG). Solid and broken lines indicate the means ± 2 SD.

sounds and breathing movement between 4 sleeping positions (supine, prone, right or left side down) were not large enough to disturb template search analysis to detect cardiac and breathing intervals.

Brief analysis showed comparable performance of the PZT sensor for HR/BR detection to ECG/IPG when neonates were stable. Average cross-correlation coefficients and differences between the cardiac interval detected by the PZT sensor system and ECG were 0.92 ± 0.12 and −0.014 ± 0.035 ms (n = 27), respectively (table 2; fig. 4), and those between the breathing interval detected by the PZT sensor system and IPG were 0.95 ± 0.02 and −0.25 ± 1.45 ms (n = 11), respectively (table 3; fig. 5). Bland-Altman plots showed that 96.8 ± 2.0 and 95.2 ± 2.2% of plots of differences in cardiac and breathing intervals, respectively, fell within ±2 SD of their mean values (tables 2, 3; fig. 4b, 5b). In addition, cross-correlation plots of an ELBW patient markedly aggregated with small HR variation (fig. 4a; open triangles).

Long assessment of HR and BR detection by the PZT sensor was also successful when the body movement of a neonate was small and infrequent (fig. 3); however, the measurement was often disturbed by body movements, mechanical ventilation, routine care and breastfeeding by the mother, etc., some of which required the neonate to be held by the mother or nurses, and consequently ECG electrodes became dislodged. These interferences impaired heart sounds and breathing movement signals as well as ECG and IPG (fig. 6). The HR detection rate by the PZT sensor and ECG in all 27 neonates examined was 82.6 ± 12.9 and 91.8 ± 4.1% (p = 0.001), respectively, while comparable in ~70% (18/27; from top in table 2) of measurements (90.2 ± 4.1 vs. 92.0 ± 3.4%; p = 0.078, Student's paired t test; p = 0.054, Wilcoxon signed rank test).

Similarly, the BR detection rates in 11 neonates are summarized in table 3. The BR detection rates obtained by the PZT sensor system and IPG were 95.9 ± 4.0 and 95.3 ± 3.5%, respectively (p = 0.38, Student's paired t test; p = 0.15, Wilcoxon signed rank test), during the period with fewer motion artifacts and other extrinsic disturbances. % time of the period was 76.0 ± 12.5 and 77.1 ± 13.5% (p = 0.86, Student's paired t test) of the total time of PZT and IPG recording, respectively. Short periods of

Table 2. Long (1–9 days) period assessment of HR detection rate (total time of successful HR detection/total measurement time) in PZT sensor measurement (PZT) and ECG, and brief (1 min) assessment of correlation coefficient and difference of cardiac interval between the PZT sensor measurement and ECG

Patient No.	Sex	Long period assessment			Brief assessment				Body weight g
		HR detection rate		duration of measurement days	average HR beats/min	correlation coefficient r	difference ± SD ms	number of plots < ±2 SD, %	
		PZT, %	ECG, %						
1	M	97.1	88.7	3	124	0.981	−0.032 ± 2.72	98.4	2,222
2	F	95.5	96.9	7	132	0.892	−0.136 ± 3.89	94.7	1,272
3	M	94.6	92.6	7	125	0.986	−0.000 ± 1.73	93.7	1,555
4	F	94.2	93.0	7	143	0.993	0.007 ± 1.12	96.5	1,582
5	M	94.0	96.0	8	141	0.986	0.014 ± 1.18	100	1,287
6	M	94.0	86.3	1	125	0.979	−0.000 ± 1.67	96.8	2,182
7	M	93.6	91.3	7	165	0.828	−0.109 ± 2.63	98.8	1,252
8	F	91.6	96.1	7	111	0.983	−0.000 ± 2.99	97.7	1,835
9	M	90.4	94.2	7	149	0.984	0.013 ± 1.33	98.8	2,082
10	M	89.8	94.1	3	126	0.997	0.016 ± 1.74	96.9	2,392
11	M	87.7	91.9	5	132	0.999	−0.015 ± 1.55	97.0	2,617
12	F	87.5	92.0	3	129	0.906	−0.000 ± 1.38	97.7	4,126
13	F	86.9	89.8	3	146	0.834	0.014 ± 1.40	97.3	1,960
14	F	86.3	97.4	9	180	0.432	−0.011 ± 1.66	95.8	912
15	M	86.0	89.9	4	131	0.921	0.008 ± 1.15	100	2,307
16	M	86.0	96.6	7	157	0.947	−0.000 ± 1.21	96.1	2,140
17	M	85.5	92.7	4	116	0.970	−0.017 ± 2.44	91.7	1,555
18	F	83.9	86.1	3	142	0.955	0.000 ± 1.51	96.5	1,932
19	F	82.3	87.8	4	130	0.991	−0.023 ± 2.27	95.4	3,496
20	M	77.2	88.2	5	142	0.941	0.007 ± 1.01	97.3	1,422
21	M	72.6	97.5	1 (10 h)	115	0.992	−0.035 ± 2.96	98.3	2,718
22	M	71.1	86.2	3	148	0.929	−0.020 ± 1.37	95.3	3,437
23	M	68.5	85.4	5	133	0.987	−0.038 ± 2.06	98.5	2,516
24	M	66.5	88.2	6	145	0.973	−0.000 ± 1.13	96.6	2,288
25	M	62.1	97.1	7	165	0.666	−0.026 ± 1.65	94.0	742
26	M	57.0	86.4	7	140	0.992	−0.014 ± 1.84	94.4	1,856
27	M	47.9	96.5	8	166	0.914	0.013 ± 1.48	98.8	1,047

breathing cessation (apnea) and irregular breathing were comparably detected by the PZT sensor and IPG during long measurement (fig. 6a, left lower; 6b, right).

Bradycardias of <80 beats/min for >5 s (fig. 7) and apneas for >15 s (fig. 6a, left lower) were found in 6/27 and 5/11 neonates, respectively. False negatives in the bradycardias were 4% (4/44 in 5 of the 6 neonates; 1 deselected patient was ventilated with high frequency oscillation (HFO) and showed false negatives of 82% due to signal contamination; fig. 8), and among apneas false negatives were found in 1 case (6%; 1/17 in 5 neonates) due to weak signal intensity. In addition, total dislodging time of ECG electrodes in the 27 and 11 neonates during long measurement was 3,362 ± 1,893 s (0.8 ± 0.4%) and 3,547 ± 3,141 s (1.2 ± 0.8%), respectively.

Interference of the PZT sensor with neonates was not perceivable as the difference in % time of body movements between measurements by the PZT sensor with ECG (24.0 ± 12.5%) and those by ECG alone (22.9 ± 13.5%) was not significant (n = 10; p = 0.86, Student's unpaired t test; p = 0.92, Mann-Whitney U test; fig. 9). Although complications were diagnosed only in the PZT sensor group, the result may be not biased because the amounts of motility of 3 patients with complications were near the middle of the list (3rd, 6th and 7th). In addition, the fact that extrinsic artifacts due to treatment by physicians and nurses or parents may have been included in the motion artifacts was not considered in this analysis. In all 69 neonates who underwent the measurement with the PZT sensor, there was no skin damage with severity

Table 3. Long (1–4 days) period assessment of BR detection rate (total time of successful BR detection/total measurement time) in PZT sensor measurement (PZT) and impedance pneumography (IPG), and brief (1 min) assessment of correlation coefficient and difference of breathing interval between the PZT sensor measurement and IPG

Patient No.	Sex	Long period assessment					Brief assessment				Body weight g
		BR detection rate		non-move time		duration of measurement days	average BR beats/min	correlation coefficient r	difference (mean ± SD) ms	plots <±2SD %	
		PZT, %	IPG, %	PZT, %	IPG, %						
1	F	99.2	99.1	69.2	73.9	2	39	0.94	−0.26 ± 43	5.1	1,917
2	M	99.0	99	72.8	73.3	3	39	0.96	−1.28 ± 42	2.6	1,755
3	F	98.0	95.6	68.8	62.8	3	52	0.93	0.96 ± 45	3.8	2,232
4	M	98.0	96.3	75.1	65.4	4	58	0.93	0.00 ± 45	8.6	2,146
5	F	97.9	98.6	66.8	61.3	4	28	0.95	3.93 ± 70	3.6	1,236
6	F	97.8	97.3	71.1	76.2	4	82	0.93	0.13 ± 27	1.2	2,852
7	M	96.5	95.6	75.5	77.8	3	67	0.92	0.90 ± 40	4.5	2,288
8	M	95.9	95.3	76.9	81.4	1	56	0.98	−0.89 ± 32	7.1	2,157
9	F	94.0	93.7	72.9	77.7	4	61	0.99	−0.56 ± 9	4.8	2,630
10	M	92.9	89	70.8	67.0	4	46	0.98	−0.43 ± 45	6.5	1,117
11	F	85.3	89.1	70.6	75.6	4	45	0.94	0.21 ± 30	4.4	3,316

Non-move time = Total time of periods with no large signal perturbation during measurement.

of stages I, II and III, from slight erythema to an abrasion [1], at sides (right/left), back or chest/abdomen. Moreover, the PZT sensor did not disturb the arrangement of other tubes or catheters attached to the neonate or the routine work of physicians and nurses.

Discussion

Cardiorespiratory monitoring by the proposed PZT sensor is likely to be highly noninvasive for neonates, as the PZT sensor caused no skin damage and did not increase body movement (fig. 9) as an index of discomfort [10–12]. Physicians who performed PZT sensor measurement did not perceive any difference in the attitude of neonates with and without the PZT sensor, although a small stress due to the PZT sensor may have been masked by the many tubes, catheters and adhesive plasters attached to a neonate. Accordingly, the thin-shaped PZT sensor with several holes, which never comes into contact with the neonate's skin, may be suitable for keeping a neonate comfortable during long-term cardiorespiratory monitoring in an incubator (fig. 1).

Brief assessment of HR and BR detection showed that the PZT sensor has an inherently high performance comparable to ECG and IPG (r = 0.92 and 0.95), consistent with a previous study in mice [7]. In addition, aggregated plots of the HR of an ELBW patient (fig. 4a; open triangles) suggest that the PZT sensor can also be used to analyze HR variability, which has been considered to be a prognostic risk indicator of life-threatening diseases including sudden infant death syndrome (SIDS).

Long assessment of PZT sensor measurements again showed a high HR detection rate (~90%) comparable to ECG in a large part (18/27) of the measurements (table 2). While, a small group (5/27) showed a lower HR detection rate of <70% (68.5–47.9%), although it was not continuously low throughout the measurement, but it was >80% for 1–2 days in 3 of 5 neonates. The lower HR detection rate was due to HFO ventilation in 2 neonates, frequent body movements in 1 neonate and weak signal intensity in another one (being transferred from a closed incubator to an open cot may have been the cause in 1 neonate). In addition, frequent changes of sleeping position among neonates might have influenced the HR detection rate. Since these lower HR detection rates might have been higher if the PZT signal had been displayed continuously on a monitor screen and sufficient attention to the sensor settings had been paid by physicians or nurses, and since the false-negative value in bradycardia detection was low (4%), the capacity of the PZT sensor for long HR measurement is probably sufficient for practical use in the NICU.

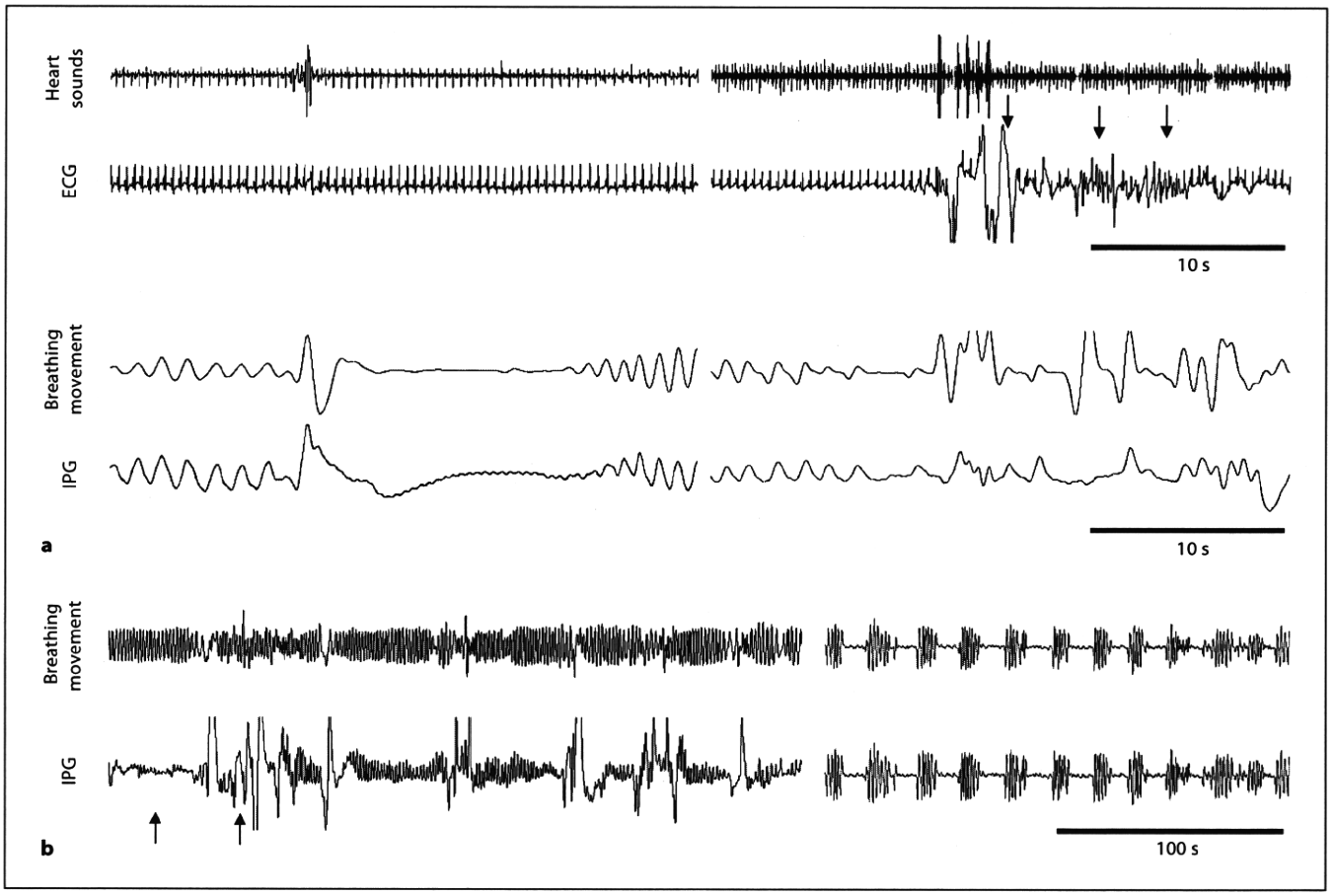

Fig. 6. Signal perturbations appeared during the simultaneous measurement of PZT sensor system and ECG/IPG. **a** From top to bottom: heart sounds obtained by the PZT system, ECG, breathing movement obtained by the PZT system and impedance pneumography (IPG). Each 4 signals in the left and right half-panels were recorded simultaneously. Left panel shows signal perturbations in heart sounds and ECG induced by a brief cessation (~15 s) of breathing (apnea; lower 2 traces). Right panel shows signal perturbations induced by a large body movement. S_1 signal is dominant in the heart sounds in the left panel, while S_1 and S_2 in the right panel are comparable. Several R waves in ECG are inarticulate compared to the S_1 and S_2 (arrows) during the body movement. **b** Signal perturbation in IPG signal was often larger than in PZT sensor signal, i.e., breathing movement (left). Breathing signal was often inarticulate in IPG (arrows) in contrast to PZT sensor signal. Irregular breathing pattern was similarly detected by both methods (right).

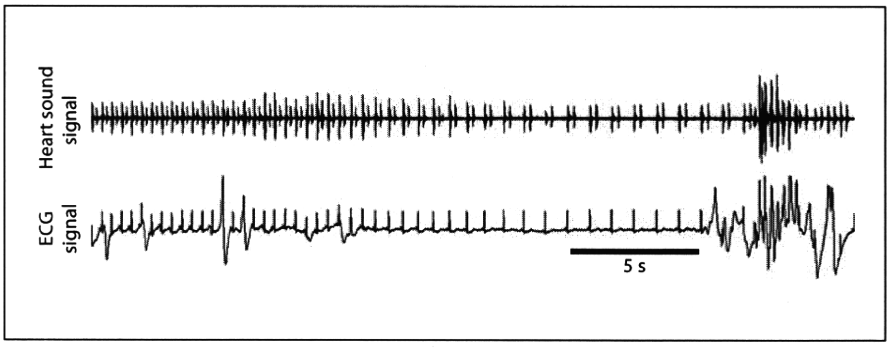

Fig. 7. Representative traces of bradycardia recorded by the PZT sensor system (upper) and ECG (lower). Heart sounds and R waves were clearly detected, and both cardiac intervals were gradually increased until a body movement emerged.

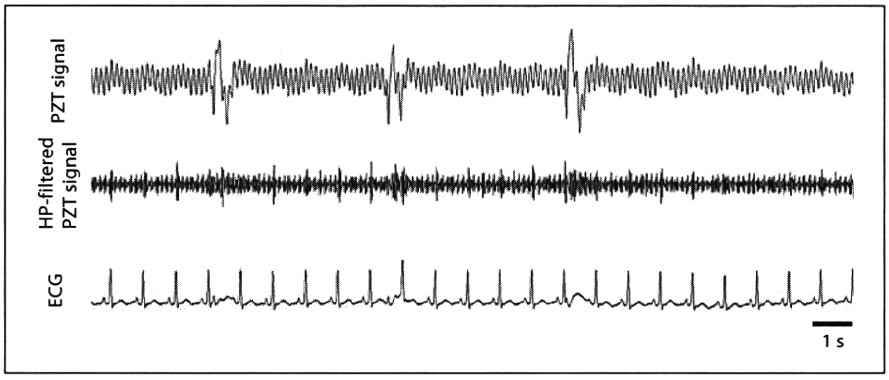

Fig. 8. PZT sensor output signal (PZT signal) influenced by mechanical ventilation (high frequency oscillation, HFO). The signal is severely contaminated with artifact of HFO (upper trace). High-pass (HP) filtering reduced the noise and several S_1 peaks are distinguishable by human eyes (middle trace), which corresponded to R waves in ECG (lower trace), but not by automatic template search analysis.

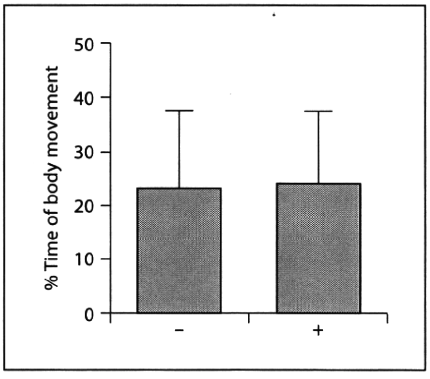

Fig. 9. Effect of PZT sensor placement on body movements of neonates. There was no significant difference in the mean (±SD) %time of body movement between neonates with (+) and without (–) the PZT sensor (n = 10, p = 0.86, Student's unpaired t test).

Cardiac monitoring by the PZT sensor provides us additional information on a lower frequency range, complimenting information obtained by a conventional stethoscope, which was developed by Laennec in 1819 [13]. The lower frequency signal that probably represents gross heart movement (fig. 2; arrows) may have useful information for clinical diagnoses [Sato et al., unpublished data] in addition to heart murmurs and accentuated second sounds [14–16]. Visualized heart and lung sound signals may contribute to increasing the detection rate of cardiac function anomalies, excluding innocent heart murmurs [15–19]. It may also be possible to predict an adverse neurologic outcome at 1 year of age by analyzing abnormal general movements [20–23], which can be detected by the PZT sensor.

It was reported that respiratory activity monitoring by a similar PZT sensor was in good agreement with that by a CO_2 respiratory monitor [24] or a thermistor airflow sensor [7] in mice. However, a large deformation of respiratory signal due to motion artifacts, routine care and artificial ventilation made BR evaluation impossible in about 30% of the total recording time in the present study (table 3). Respiratory-signal deformation is also a recognized problem in IPG [25–29] (fig. 6a, right; 6b, left lower). As a consequence, the BR detection rate was compared between the PZT sensor and IPG using ~70% of total data, which resulted in considerably good agreement (fig. 5; table 3). As the impairment of respiratory signals often occurred either in the PZT signal or IPG but not always at the same time (fig. 6b, left lower, arrows), respiratory monitoring with both a PZT sensor and IPG might reduce the false alarms that often disturb nurses in the NICU. In addition, as both methods detect different information on respiratory activity from different sites on a neonate's body, it might be of help in discriminating between central sleep apnea and obstructive sleep apnea [Sato et al., unpublished data], and also in studying sudden infant death syndrome [30].

In the present study, long-term assessment was limited by compromised evaluation due to the huge data size. Nonetheless, according to the comparable HR detection rate (difference 0.4%) in a representative 10,000 s data between automatic analysis with and without a thorough manual verification, we believe that errors in HR/BR detection rate with the simplified manual verification were mostly within ± 1%. A more practical assessment will be performed after manufacturing a real-time PZT sensor-based cardiorespiratory monitor for newborns in the NICU.

Many types of other PZT sensors for cardiorespiratory monitoring have been proposed. They are generally susceptible to motion and have disadvantages for use in the

NICU; for example, a mattress-type sensor seems to be difficult to handle in an incubator, to sterilize and let babies sleep comfortably. In contrast, our PZT sensor was made as small as possible to impede motion artifacts from a wider area, and a form mattress under the PZT sensor attenuates extrinsic vibration from the floor propagating through the bed frame of an incubator, although the artifact of HFO is still unavoidable. The influence of the HFO on heart sound signal should be resolved by advanced signal-processing algorithms such as pattern recognition, wavelet transforming or independent component analysis [17, 31, 32] since the human eye can distinguish S_1 from HFO noise (fig. 8, middle trace). The PZT sensor also showed strong durability for repetitive use of over 12 months; it is easy to handle, to sterilize and to use over a long duration without changing the sensor because it causes no skin irritation and because one does not have to worry about wet-gel drying up that deteriorates signal quality when using ECG electrodes.

In addition, we often observed a loss of ECG/IPG signal for several to 10 s of minutes although the PZT sensor signal recorded continuously, which suggests that the two systems can help each other when either one fails to detect a signal. Accordingly, the PZT sensor system can be used as a backup cardiorespiratory monitor for a more secure monitor system, or as a main cardiorespiratory monitor for a healthier infant who does not necessarily require full ECG information. Furthermore, the system may serve well as an advanced diagnostic tool for cardiac diseases because it utilizes the PZT system and analyzes information derived from both acoustic cardiography and ECG [15, 16, 18].

In conclusion, the PZT sensor is noninvasive and does not cause skin irritation, but we believe it does provide reliable, accurate measurements for monitoring of long-term cardiorespiratory activity of neonates in the NICU, although the issue of mechanical ventilation noise (HFO in particular) remains to be solved.

Acknowledgements

This work was supported in part by the Vehicle Racing Commemorative Foundation, Unique Medical Co., Ltd., Fukuda Denshi Co., Ltd., AT Labo Co., Ltd. and an intramural grant from Akita University School of Medicine. The authors thank the staff of the NICU at Akita University Hospital, and Kumi Sato and Qing Liu for their technical contributions to data analysis.

References

1 Barak M, Hershkowitz S, Rod R, Dror S: The use of a synthetic skin covering as a protective layer in the daily care of low birth weight infants. Eur J Pediatr 1989;148:665–666.

2 Di Rienzo M, Rizzo F, Meriggi P, Bordoni B, Brambilla G, Ferratini M, Castiglioni P: Applications of a textile-based wearable system for vital signs monitoring. Conf Proc IEEE Eng Med Biol Soc 2006;1:2223–2226.

3 Brouillette RT, Morrow AS, Weese-Mayer DE, Hunt CE: Comparison of respiratory inductive plethysmography and thoracic impedance for apnea monitoring. J Pediatr 1987;111:377–383.

4 DeGroff CG, Bhatikar S, Hertzberg J, Shandas R, Valdes-Cruz L, Mahajan RL: Artificial neural network-based method of screening heart murmurs in children. Circulation 2001;103:2711–2716.

5 Kleinman CS: Cardiac ultrasonography in the fetus and newborn. Mead Johnson Symp Perinat Dev Med 1987;25:32–39.

6 Ommen SR, Nishimura RA, Appleton CP, Miller FA, Oh JK, Redfield MM, Tajik AJ: Clinical utility of Doppler echocardiography and tissue Doppler imaging in the estimation of left ventricular filling pressures: a comparative simultaneous Doppler-catheterization study. Circulation 2000;102:1788–1794.

7 Sato S, Yamada K, Inagaki N: System for simultaneously monitoring heart and breathing rate in mice using a piezoelectric transducer. Med Biol Eng Comput 2006;44:353–362.

8 Sato S: Cardiac beat detector – a novel analogue circuitry for the first heart sound discrimination. Biosignals Proc 2008;2:136–140.

9 Sato S: Quantitative evaluation of ontogenetic change in heart rate and its autonomic regulation in newborn mice with the use of a noninvasive piezoelectric sensor. Am J Physiol Heart Circ Physiol 2008;294:H1708–H1715.

10 Ratcliffe JM: Sedation in the intensive care unit. Curr Pediatr 1994;4:106–109.

11 Playfor SD, Thomas DA, Choonara I, Collier J, Jarvis A: Parental perceptions of comfort during mechanical ventilation. Paediatr Anaesth 2001;11:99–103.

12 Hadjistavropoulos HD, Craig KD, Grunau RE, Whitfield MF: Judging pain in infants: behavioural, contextual, and developmental determinants. Pain 1997;73:319–324.

13 Noonan JA: A history of pediatric specialties: the development of pediatric cardiology. Pediatr Res 2004;56:298–306.

14 Levi DS, Kusnezov N, Carman GP: Smart materials applications for pediatric cardiovascular devices. Pediatr Res 2008;63:552–558.

15 Larkin M: Paediatric heart sounds assessed by computer. Lancet 2001;357:1856.

16 Erne P: Beyond auscultation – acoustic cardiography in the diagnosis and assessment of cardiac disease. Swiss Med Wkly 2008;138:439–452.

17 Debbal SM, Bereksi-Reguig F: Computerized heart sounds analysis. Comput Biol Med 2008;38:263–280.

18 Noponen AL, Lukkarinen S, Angerla A, Sepponen R: Phono-spectrographic analysis of heart murmur in children. BMC Pediatr 2007;7:23.

19 Smith KM: The innocent heart murmur in children. J Pediatr Health Care 1997;11:207–214.

20 Lüchinger AB, Hadders-Algra M, van Kan CM, de Vries JI: Fetal onset of general movements. Pediatr Res 2008;63:191–195.

21 Hadders-Algra M, Mavinkurve-Groothuis AM, Groen SE, Stremmelaar EF, Martijn A, Butcher PR: Quality of general movements and the development of minor neurological dysfunction at toddler and school age. Clin Rehabil 2004;18:287–299.

22 Prechtl HF, Einspieler C, Cioni G, Bos AF, Ferrari F, Sontheimer D: An early marker for neurological deficits after perinatal brain lesions. Lancet 1997;349:1361–1363.
23 Groen SE, de Blecourt AC, Postema K, Hadders-Algra M: General movements in early infancy predict neuromotor development at 9 to 12 years of age. Dev Med Child Neurol 2005;47:731–738.
24 Miyake A, Yamada K, Kosaka T, Miki T, Seino S, Inagaki N: Disruption of Kir6.2-containing ATP-sensitive potassium channels impairs maintenance of hypoxic gasping in mice. Eur J Neurosci 2007;25:2349–2363.
25 Khambete ND, Brown BH, Smallwood RH: Movement artefact rejection in impedance pneumography using six strategically placed electrodes. Physiol Meas 2000;21:79–88.
26 Ernst JM, Litvack DA, Lozano DL, Cacioppo JT, Berntson GG: Impedance pneumography: noise as signal in impedance cardiography. Psychophysiology 1999;36:333–338.
27 Cohen KP, Ladd WM, Beams DM, Sheers WS, Radwin RG, Tompkins WJ, Webster JG: Comparison of impedance and inductance ventilation sensors on adults during breathing, motion, and simulated airway obstruction. IEEE Trans Biomed Eng 1997;44:555–566.
28 Rosell J, Webster JG: Signal-to-motion artifact ratio versus frequency for impedance pneumography. IEEE Trans Biomed Eng 1995;42:321–323.
29 Adams JA, Zabaleta IA, Stroh D, Sackner MA: Measurement of breath amplitudes: comparison of three noninvasive respiratory monitors to integrated pneumotachograph. Pediatr Pulmonol 1993;16:254–258.
30 Ramanathan R, Corwin MJ, Hunt CE, Lister G, Tinsley LR, Baird T, Silvestri JM, Crowell DH, Hufford D, Martin RJ, Neuman MR, Weese-Mayer DE, Cupples LA, Peucker M, Willinger M, Keens TG: Cardiorespiratory events recorded on home monitors. JAMA 2001;285:2199–2207.
31 Nazeran H: Wavelet-based segmentation and feature extraction of heart sounds for intelligent PDA-based phonocardiography. Methods Inf Med 2007;46:135–141.
32 Matsumoto M, Hashimoto S: An acoustical array combining microphones and piezoelectric devices. J Acoust Soc Am 2008;123:2117–2125.